



1 **Global Nitrogen and Sulfur Budgets Using a Measurement-**
2 **Model Fusion Approach**

3 **Hannah J. Rubin¹, Joshua S. Fu^{1,2}, Frank Dentener³, Rui Li⁴, Kan Huang⁵, Hongbo Fu⁵**

4 ¹Department of Civil and Environmental Engineering, University of Tennessee, Knoxville, TN, 37996, USA

5 ²Computational Earth Science Group, Oak Ridge National Laboratory, Oak Ridge, TN 37831, USA

6 ³European Commission, Joint Research Centre, Ispra, Italy

7 ⁴Ministry of Education Key Laboratory for Earth System Modeling, Department of Earth System Science, Tsinghua
8 University, Beijing, 100084, China

9 ⁵Shanghai Key Laboratory of Atmospheric Particle Pollution and Prevention (LAP3), Department of Environmental
10 Science and Engineering, Fudan University, Shanghai, 200433, China

11
12 E-mail: jsfu@utk.edu

13
14 **Keywords:** Measurement-model fusion, nitrogen deposition, sulfur deposition, HTAP II,
15 ammonia, multiple-model mean

16



17 **Abstract**

18 Global reactive nitrogen (N) deposition has more than tripled since 1860 and is expected to
19 remain high due to land use changes and fossil fuel consumption. We update the 2010 global
20 deposition budget for nitrogen and sulfur with new regional wet deposition measurements from
21 Asia, improving the ensemble results of eleven global chemistry transport models from the
22 second phase of the United Nation's Task Force on Hemispheric Transport of Air Pollution
23 (HTAP-II). The observationally adjusted global N deposition budget is 130 Tg-N, representing a
24 10% increase and the adjusted global sulfur deposition budget is 80 Tg-S, representing no
25 change. Our study demonstrates that a global measurement-model fusion approach can
26 substantially improve N and S deposition model estimates at a regional scale and represents a
27 step forward toward the World Meteorological Organization's goal of global fusion products for
28 accurately mapping harmful air pollution.

29

30 **1. Introduction**

31 Atmospheric nitrogen and sulfur deposition from human activities related to the use of fossils
32 and land use have significant implications for ecosystem and human health (Bobbink et al.,
33 2010). Elevated levels of nitrogen and sulfur can lead to eutrophication (Anderson et al., 2008;
34 Heisler et al., 2008), changes in carbon sequestration (Kicklighter et al., 2019; de Vries et al.,
35 2009; Zhu et al., 2020), loss of biodiversity (Clark et al., 2013; Dise and Stevens, 2005), and
36 acidification (Bowman et al., 2008). While sulfur deposition is expected to decrease over the
37 next 80 years (Lamarque et al., 2013), it will remain a serious hazard in many emerging
38 economies. For instance, sulfur deposition in East Asia peaked in 2006 (Lu et al., 2010) but is
39 still high enough to be concerning, especially in natural and semi-natural regions (Doney et al.,
40 2007; Luo et al., 2014).

41 Oxidized nitrogen (NO_y) and reduced nitrogen (NH_x), together called reactive nitrogen (Nr), and
42 oxidized sulfur (SO_x) deposition occur as wet and dry processes (Dentener et al., 2006). Wet
43 deposition is measured at hundreds of locations in Europe, North America, and Asia, but dry
44 deposition is harder to measure and is often instead derived from ambient concentrations and
45 modeled deposition velocities (Xu et al., 2015). It is measured continuously at a few locations in



46 North America (Clean Air Status and Trends Network (CASTNET), 2021) and Asia (Acid
47 Deposition Monitoring Network in East Asia (EANET), 2021).

48 The United Nations Economic Commission for Europe’s Task Force on Hemispheric Transport
49 of Air Pollution (HTAP) is an international effort to improve the understanding of air pollution
50 transport science with emissions models. The second phase of HTAP was launched in 2012. Tan
51 et al. (Tan et al., 2018) used the multi-model mean (MMM) of 11 HTAP II chemistry transport
52 models to estimate the sulfur and nitrogen deposition budgets for 2010. Significant uncertainty
53 remained due to a lack of station measurements, especially in East Asia, a large contributor to the
54 overall budget. Tan et al. (Tan et al., 2018) compared Acid Deposition Monitoring Network in
55 East Asia (EANET (Acid Deposition Monitoring Network in East Asia (EANET), 2021))
56 measurements to the MMM output but there were very few measurements in East Asia and all
57 were located along the southeastern coast. In contrast, the highest emissions and modeled
58 deposition were inland and north, making it challenging to evaluate model performance.

59 Combining measurements and model estimates in a “measurement-model fusion” (MMF)
60 approach has the advantage of retaining the broad spatial coverage of models while accurately
61 matching observations. Generally speaking, MMF takes model estimates for a region and
62 modifies them based on in-situ point measurements of the phenomenon to “nudge” the model
63 towards the observed values (Labrador et al., 2020). One global MMF approach for wet
64 deposition combined measurements with HTAP I ensemble model values for 2000-2002 (Vet et
65 al., 2014) where model estimates filled empty grid cells lacking a 3-year observed mean.

66 Another MMF approach in North America (Atmospheric Deposition Analysis Generated from
67 optimal Interpolation from Observations, “ADAGIO”) used observed concentrations to adjust
68 predicted concentrations from the Global Environmental Multiscale-Modelling Air Quality and
69 Chemistry (GEM-MACH) model (Schwede et al., 2019). Recent work in the US (Schwede and
70 Lear, 2014; Zhang et al., 2019) incorporates Community Multiscale Air Quality (CMAQ) model
71 output and precipitation data generated by the Parameter-elevation Regressions on Independent
72 Slopes Model (PRISM, <https://prism.oregonstate.edu/>, Accessed: 10/01/22), as well as
73 observations using inverse distance weighting to create total deposition (“TDep”,
74 <https://nadp.slh.wisc.edu/committees/tdep/#tdep-maps>) maps that are publicly available.



75 More details of the MMF approach are described in Fu et al. (Fu et al., 2022) as they lay out a
76 roadmap for future work, following the World Meteorological Organization's Global
77 Atmosphere Watch Program (WMO GAW) and the intended role of the MMF Global Total
78 Atmospheric Deposition (MMF-GTAD) project. This study updates Tan et al.'s (Tan et al.,
79 2018) global S and N deposition budgets using a variation of the TDep methodology (Schwede
80 and Lear, 2014) to merge NH_x , NO_y , and SO_x gridded surfaces from modeled results with
81 observations of NO_3^- , NH_4^+ , and SO_4^{2-} in precipitation and as an aerosol. We demonstrate the
82 viability of a straightforward but globally applicable MMF approach while remaining consistent
83 with previous work that provides impact assessments for various communities. This approach is
84 an essential step towards the WMO's goal of reliable deposition products to aid decision-making.
85 We update the 2010 deposition budgets using MMF to combine the broad spatial coverage of a
86 model with accurate in-situ measurements. The total nitrogen deposition budget is recalculated to
87 130 Tg-N and the sulfur budget is 80 Tg-N, representing about a 10% increase and no change,
88 respectively, from the modeled values.

89 **2. Data Availability**

90 All data are from 2010, collected monthly. Wet deposition measurements (NO_3^- , NH_4^+ , and
91 SO_4^{2-}) from the US's National Trends Network (NTN) and Atmospheric Integrated Research
92 Monitoring Network (AIRMoN) are available through the National Atmospheric Deposition
93 Program (NADP (National Atmospheric Deposition Program, 2021),
94 <http://nadp.slh.wisc.edu/NTN/>). Measurements were filtered for completeness and quality,
95 following Schwede and Lear (Schwede and Lear, 2014). Sites without a full year of
96 measurements or with quality tags indicating collection issues were not included, resulting in 247
97 observations. Dry deposition generated values are available from the Clean Air Status and
98 Trends Network (CASTNET (Clean Air Status and Trends Network (CASTNET), 2021)) at 84
99 locations. CASTNET uses an inferential method to calculate dry deposition fluxes as a product
100 of surface concentration and modeled dry deposition velocity.
101 Nitrogen and sulfur wet deposition measurements and dry deposition estimates throughout
102 Canada are recorded by the Canadian Air and Precipitation Monitoring Network (CAPMoN
103 (Canadian Air and Precipitation Monitoring Network, 2021)) and are available through the
104 National Atmospheric Chemistry (NAtChem) database
105 (<https://donnees.ec.gc.ca/data/air/monitor/>). Dry deposition estimates from CAPMoN are



106 calculated by multiplying atmospheric concentration and deposition velocity. There were 27 sites
107 with a full year of data.

108 The European Monitoring and Evaluation Programme (EMEP (European Monitoring and
109 Evaluation Programme (EMEP), 2021; Tørseth et al., 2012), <http://ebas-data.nilu.no/>) has records
110 of precipitation chemistry (NO_3^- , NH_4^+ , and SO_4^{2-}) for Europe. There were 86 sites with a full
111 year of data.

112 A promising data set of wet deposition measurements (NO_3^- , NH_4^+ , and SO_4^{2-}) in China is
113 available through the National Nitrogen Deposition Monitoring Network (NNDMN (Xu et al.,
114 2019)). It is comparable to other regional measurements (Wen et al., 2020). However, these data
115 only exist for a fraction of 2010 (from September onwards) for a few sites; rather than use partial
116 data to represent an entire year, these sites were not included. A prior multi-year nationwide field
117 study, including some of these NNDMN data, was compiled by Li et al. (Li et al., 2019), which
118 was used in this work as a good proxy for use of NNDMN data in the future studies. Daily NO_3^- ,
119 NH_4^+ , and SO_4^{2-} site measurements (in mg/L) were averaged over the year for each of the 407
120 site locations with complete records by multiplying the concentration by the precipitation
121 recorded at that same site (in mm) and then aggregating to produce annual precipitation-
122 weighted deposition (Sirois, 1990). EANET (Asia Center for Air Pollution Research, 2021,
123 <https://www.eanet.asia/>) wet and dry deposition and precipitation data are available at 47 sites.

124 The International Global Atmospheric Chemistry (IGAC) Deposition of Biogeochemically
125 Important Trace Species (DEBITS) Africa (IDAF) program (Adon et al., 2010; Galy-Lacaux et
126 al., 2014) has NH_4^+ and NO_3^- precipitation concentrations on the International Network to Study
127 Deposition and Atmospheric Chemistry in Africa (INDAAF (INDAAF – International Network
128 to study Deposition and Atmospheric chemistry in Africa, 2021)) website ([https://indaaf.obs-
mip.fr/](https://indaaf.obs-
mip.fr/)) for one site in Niger.

130 All measurements were converted to mg-N (or S) /m².

131
132
133
134
135



136 **3. Procedure**

137 Global yearly wet and dry NO_3^- , NH_4^+ , and SO_4^{2-} deposition observations (for wet deposition) or
138 estimates (for dry deposition) were combined with the respective HTAP II model average grid
139 cell estimates, using common 1 degree x 1 degree ($1^0 \times 1^0$) grid cells (Figure 1). For example,
140 wet NO_3^- deposition observations are combined with the wet NO_3^- modeled deposition in the
141 nearest HTAP II MMM grid cell to the observation, where observations exist. Dry deposition
142 values (NO_3^- , NH_4^+ , and SO_4^{2-}) from CASTNET and n inverse-distance weighted $1^0 \times 1^0$ gridded
143 dataset was created based on the distance from each observation to the center of the nearest
144 HTAP II model grid cell. Inverse-distance weighting (IDW) was selected as the most
145 implementable method to introduce MMF on a global scale while remaining consistent with
146 previous work (Schwede and Lear, 2014).
147 The weighting function was calculated as

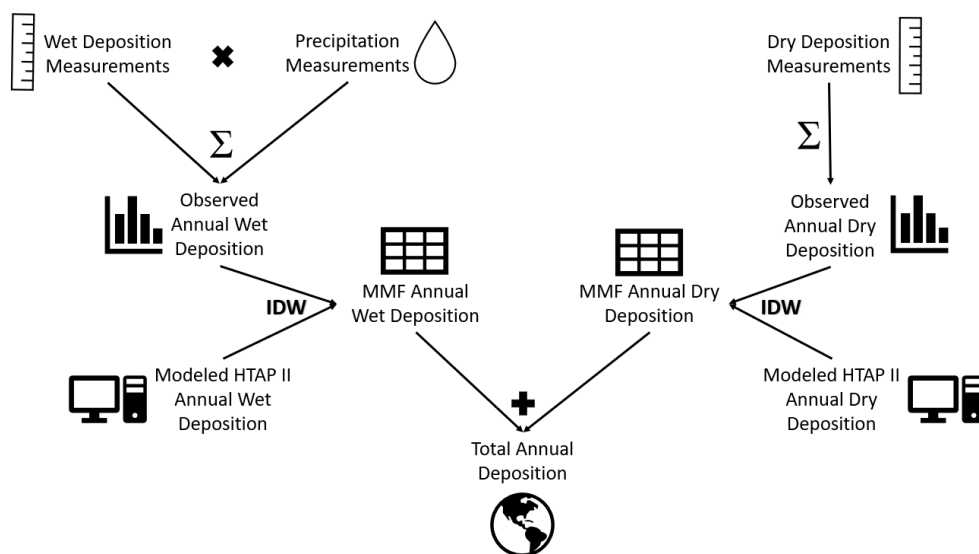
148
$$\left(1 - \frac{\text{distance}}{\text{max distance}}\right)^2 \quad (1)$$

149 following Schwede and Lear's (Schwede and Lear, 2014) approach for the TDep product, where
150 "distance" is the distance between the site location and the center of the HTAP II model grid cell
151 nearest to that sampling site location, within a maximum distance of 1^0 (approximately 111 km
152 at middle latitudes). This maximum distance was chosen because that is the resolution of the
153 HTAP II grids, not because that is the distance a species might travel in the atmosphere before it
154 is deposited. The output values of the weighting function at each observation location are then
155 multiplied by the observed deposition. For the center of every HTAP II model grid cell near that
156 site, the modeled deposition is multiplied by 1 minus the value of the weighting function. As a
157 consequence, if there are no observations near a model grid cell, the cell value remains the same.
158 The two grids ([weighting function times observed deposition] and [1-weighting function times
159 modeled deposition]) are added together. This has the effect of modifying the HTAP II grid only
160 in locations where there are observations nearby.

161 The MMF gridded surfaces were then summed by species along with the remaining unchanged
162 HTAP II gridded surfaces that lacked in-situ measurements to create total N and S deposition
163 gridded surfaces (e.g., the MMF wet and dry SO_4^- gridded surfaces were added to the HTAP II
164 wet and dry SO_2 gridded surfaces to get total S deposition). The MMF wet deposition surfaces



165 include measurements from Europe, Asia, and North America, but the dry deposition MMF
166 surface only includes measurements from the USA and Asia, due to a lack of measurements
167 elsewhere.



168

169

Figure 1. A flowchart describes the MMF methodology implemented in this paper.

170

171 **4. Results**

172 The total global NH_x deposition in 2010 is adjusted from 54 Tg-N (from HTAP II models) to
173 70.65 Tg-N (Table 1). Combined with a NO_y deposition of 59.4 Tg-N (from a modeled HTAP II
174 59.3 Tg-N), the total global deposition is adjusted to 130 Tg-N (from 113 Tg-N). Most of this
175 increase comes from a model underestimation in East Asia (Figure 2A). Total S deposition is
176 adjusted to 80 Tg-S (Table 1), a slight decrease from the HTAP II model prediction of 83.5 Tg-S
177 (Figure 2B).

178

179

180

181

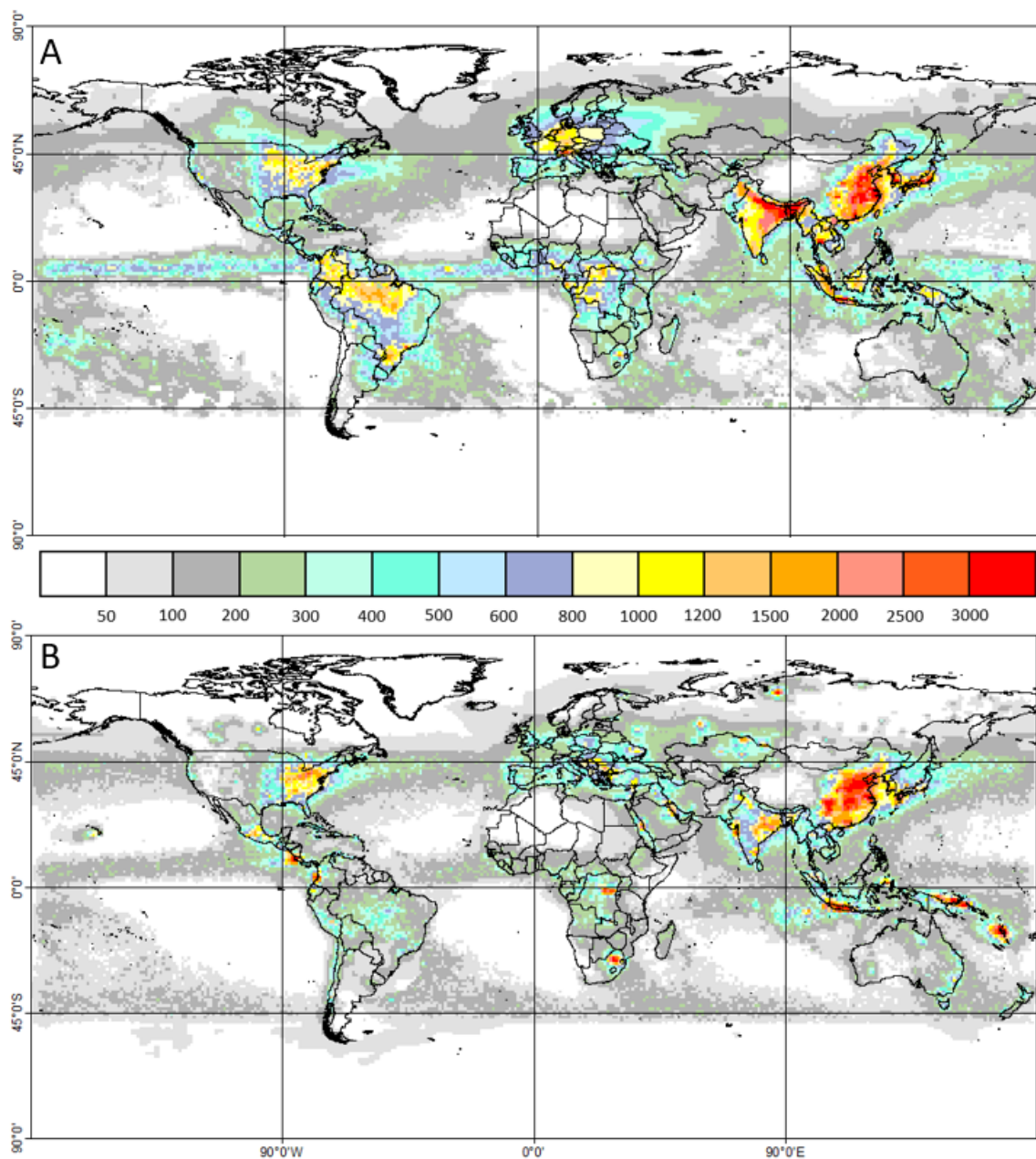
182



183 **Table 1: 2010 adjusted global wet and dry deposition in Tg**, MMM indicates Tan et al.'s 2018 multi-model mean
 184 and MMF is this measurement-model fusion work. Coastal means within 1 degree of the coastline. RBU is an
 185 abbreviation for Russia, Belarus, and Ukraine.

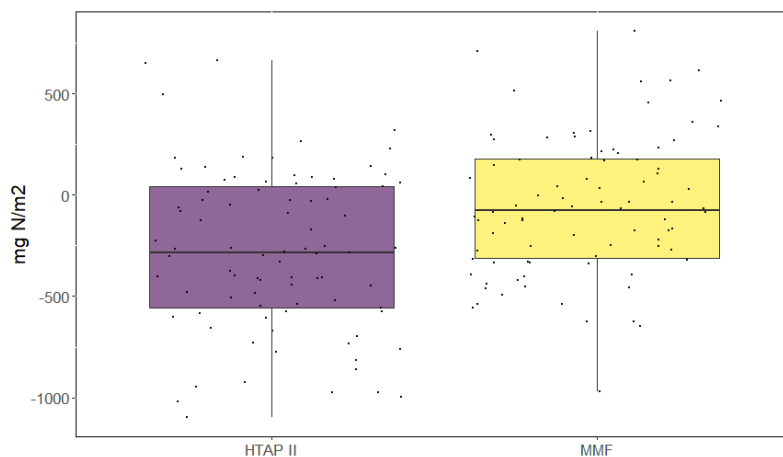
	Non-Coastal		Coastal		Non-Coastal		Coastal		Non-Coastal		Coastal	
	MMM	MMF	MMM	MMF	MMM	MMF	MMM	MMF	MMM	MMF	MMM	MMF
Region	Total NH_x				Total NO_y				Total S			
North America	3.40	4.56	0.40	1.02	4.40	4.34	0.80	1.50	4.70	3.35	1.30	1.60
Europe	2.50	1.97	0.80	1.74	2.60	1.61	1.20	1.76	2.70	1.21	1.50	1.99
South Asia	8.60	8.60	1.00	1.00	3.60	3.60	0.70	0.70	3.70	3.70	1.00	1.00
East Asia	6.70	5.93	1.00	1.84	8.30	4.85	2.20	3.47	11.20	8.04	2.90	3.69
Southeast Asia	3.20	1.13	1.60	2.87	1.90	0.74	1.40	1.67	2.40	0.71	2.80	3.51
Australia	0.40	0.40	0.40	0.40	0.60	0.60	0.40	0.40	1.00	1.00	1.50	1.50
North Africa	0.70	0.70	0.20	0.20	1.40	1.40	0.40	0.40	1.00	1.00	0.50	0.50
Sub-Saharan Africa	3.40	3.40	0.40	0.40	4.70	4.70	0.60	0.60	2.70	2.70	0.70	0.70
Middle East	0.50	0.70	0.10	0.30	1.40	1.40	0.30	0.30	1.70	1.70	0.60	0.60
Central America	1.40	1.40	0.60	0.60	1.20	1.20	0.80	0.80	1.40	1.40	1.40	1.40
South America	3.80	3.80	0.30	0.30	3.40	3.40	0.30	0.30	2.40	2.40	0.60	0.60
RBU	1.80	3.48	0.30	0.68	2.40	2.50	0.50	0.68	3.60	2.81	0.90	0.78
Central Asia	0.50	0.50	0.00	0.00	0.60	0.60	0.00	0.00	1.20	1.20	0.10	0.10
Antarctica	0.10	0.10	0.00	0.00	0.10	0.10	0.00	0.00	1.40	1.40	0.00	0.00
Continental	37.00	36.70	7.10	11.67	36.70	29.81	9.70	11.81	41.00	32.62	15.60	18.28
Open Oceans	9.90	22.28			12.90	17.80			26.90	29.10		
Global	46.90	58.98	7.10	11.67	49.60	47.61	9.70	11.81	67.90	61.72	15.60	18.28

186
187

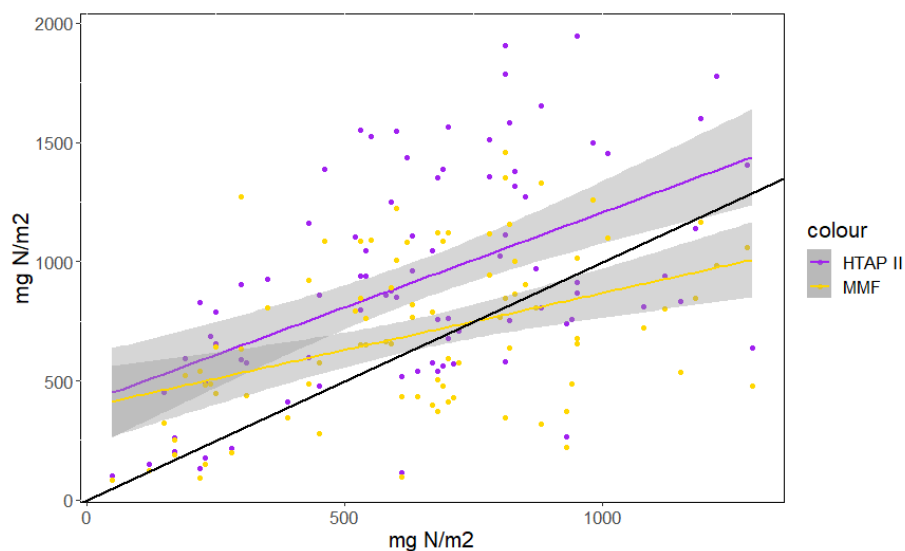


188
189
190
191
192

Figure 2: Total N and S deposition in 2010 using the MMF approach. A) Total N deposition (mg N/m²), the sum of wet and dry NO₃⁻ and NH₄⁺ after applying the MMF approach, as well as HTAP II gridded surfaces of wet and dry NH₃, HNO₃, and NO₂ with no MMF approach due to the lack of measurements. **B)** Total S deposition (mg S/m²), the sum of wet and dry MMF SO₄²⁻ and wet and dry HTAP II SO₂.



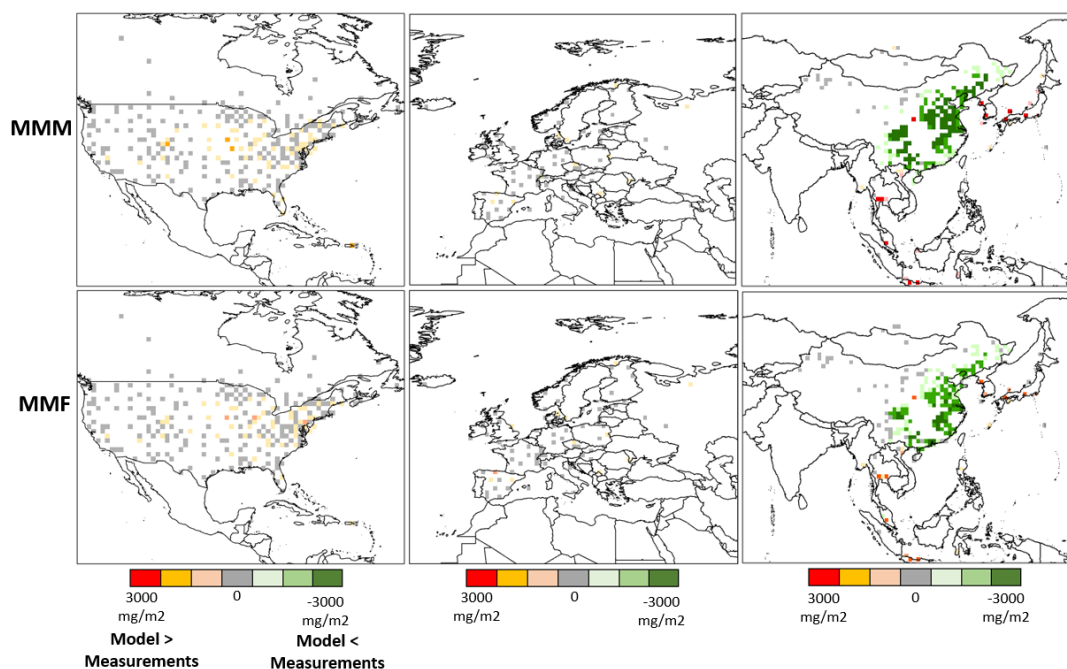
193



194

195 **Figure 3: A comparison between HTAP II and MMF results at EMEP observation sites. A)** A boxplot shows
196 the distribution of difference between EMEP and HTAP II and EMEP and MMF modeled wet deposition results at
197 each EMEP observation location. **B)** HTAP II and MMF values versus the respective EMEP wet deposition
198 observation at each measurement location with standard error shown in gray. The 1:1 line is black.

199 Tan et al. (2018) report that their MMM is underestimating the high observations of total N
200 deposition at some EMEP stations. We find that our value for European N deposition (7.08 Tg)
201 is very similar to the MMM surface (7.10 Tg), though higher observations are better reproduced
202 with MMF (Figure 3). Higher observations in East Asia are also better reproduced with MMF
203 (Figure 4).



204

205 **Figure 4. The difference between modeled and observed deposition.** Observed annual wet nitrogen deposition is
206 subtracted from MMM and MMF annual wet nitrogen deposition for North America, Europe, and Asia, respectively
207 in mg/m^2 .

208

209 The spatial distribution is slightly different, with more deposition in coastal areas in the MMF
210 estimate (Table 1). Tan et al. (Tan et al., 2018) report that the HTAP II MMM overestimates
211 NO_3^- wet deposition in North America, but underestimates NH_4^+ deposition. We find that the
212 MMF interpolated deposition slightly improves these estimates, although the spatial distribution
213 is very similar (Figures 2, 5). The largest change for N deposition (comparing MMM and MMF)
214 is in grid cells classified as ocean because of an increase in East and Southeast Asia deposition
215 which mostly occurs in areas classified as ocean due to the small island size and low spatial
216 resolution. Ocean cells were classified as such if they were located further than 1 degree from the
217 mainland; therefore, any islands smaller than 1 degree were counted as ocean. The largest change
218 for S deposition is in continental grid cells due to a decrease in East Asia.

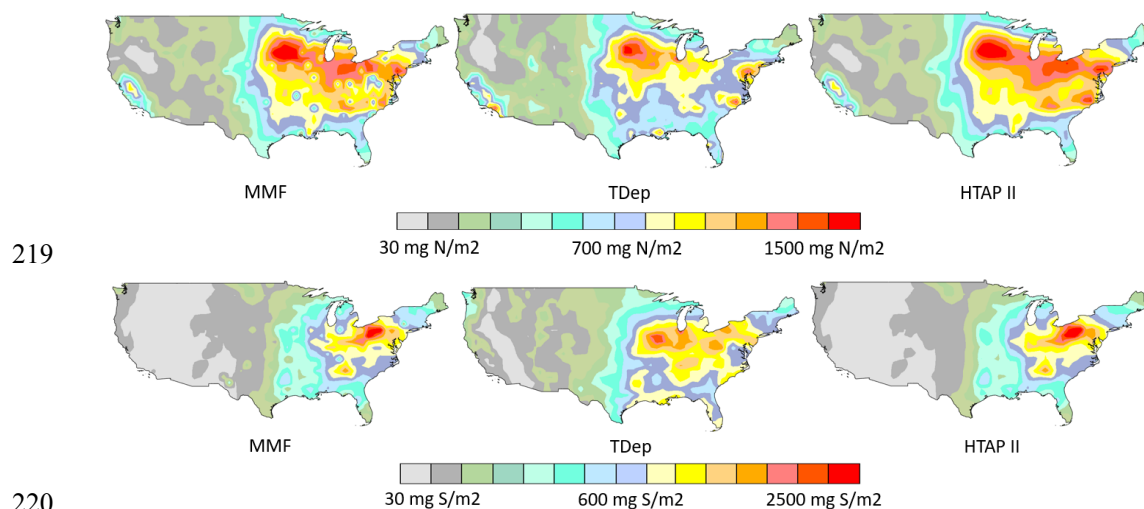
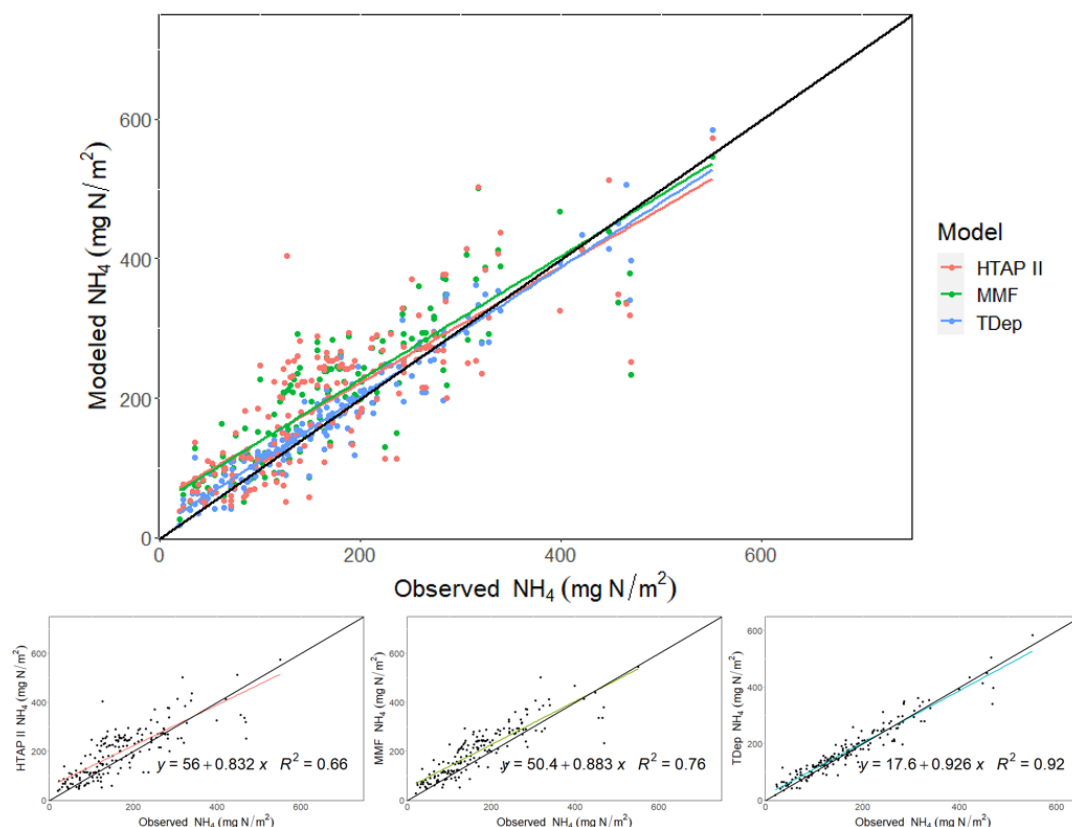


Figure 5: 2010 Total N deposition in the US. A) Total N is modeled with 1) MMF (this work), 2) TDep annual map available from the NADP and 3) Tan et al.'s 2018 MMM. B) 2010 SO_x wet deposition in the US as modeled with 1) MMF (this work), 2) TDep annual map available from the NADP, and 3) Tan et al.'s 2018 multi-model mean HTAP II output.

There are spatial differences between an aggregated $1^0 \times 1^0$ the original TDep map of nitrogen deposition for the United States as available from the NADP (Figure 5A), the HTAP II surface produced by Tan et al. (Tan et al., 2018) corresponding to the same area, and the deposition map produced in this work. A similar pattern is seen in the map of SO_4^{2-} (Figure 5B).

The R^2 value for the linear regression between MMF wet NH_4 and observed wet NH_4 in the US is 0.76 (Figure 6). The R^2 value for the linear regression between the HTAP II wet NH_4 and observed NH_4 is 0.66, and 0.92 for the linear regression between the TDep wet NH_4 and observed NH_4 (Figure 6). This means that TDep is better reproducing the NADP/NTN measurements, whereas the MMF methodology is more similar to the HTAP II model. The higher TDep R^2 value likely occurs because of the finer mesh (12 km) used in the TDep product, and the closer proximity to individual stations as compared to HTAP II used in the MMF approach. All three datasets produce similar values to the measured wet NH_x deposition at the NADP/NTN sites (Figure 6).



239

240 **Figure 6: Observed and modeled wet NH_4 deposition in the US in 2010.** Each NADP/NTN wet deposition
241 measurement and the associated HTAP II, TDep, or MMF NH_x wet deposition value. The black line is the 1:1 line.

242

243 5. Discussion

244 Geddes et al. (Geddes and Martin, 2017) used satellite observations to report global NO_y
245 emissions of 57.5 Tg-N/yr in 2010, similar to the 59.26 Tg-N emissions reported by HTAP II.
246 This matches well with our total NO_y deposition (59.4 Tg-N). However, it suggests that either
247 emissions for HTAP II models' simulations are too low, or deposition is too high since
248 presumably deposition should be similar to or lower than emissions. HTAP II ammonia
249 emissions were 51.93 Tg-N, lower than the MMF NH_3 and NH_4 deposition of 70.65 Tg-N,
250 suggesting that emissions are too low, or deposition is too high. The total MMM sulfur emissions
251 for 2010 were 90.7 Tg S, somewhat larger than the MMF sulfur deposition of 80 Tg-N.



252 Research in China (Liu et al., 2020) explored the spatial pattern of N deposition by combining
253 satellite observations with NNDMN observations (Xu et al., 2019); they found a 2012 average of
254 18.21 kg N ha⁻¹. Additional work combining the GEOS-Chem
255 (<http://acmg.seas.harvard.edu/geos/>) model with satellite observations and surface measurements
256 reports the average annual deposition from 2008-2012 as 16.4 Tg-N with 10.2 Tg-N from NH_x
257 and 6.2 Tg-N from NO_y (Zhao et al., 2017). The averages reported by these studies are consistent
258 with ours (16.6 kg · ha⁻¹ · yr⁻¹) despite the slight difference in timeframe and resolution. The
259 spatial pattern of N deposition in 2010 (Figure 2A) also remains similar to that of previous
260 decades (Jia et al., 2014), with high deposition in eastern China and low deposition over the
261 Tibetan Plateau. This pattern is confirmed in 2006 and 2013 (Qu et al., 2017).

262 As seen in Table 1, the largest difference between MMM and MMF is in the ocean. While MMF
263 does give better deposition estimates by incorporating in-situ measurements, it is worth
264 considering the scale of the model. Observations of deposition are probably not representative
265 for a 1^o resolution and observations of precipitation may not be homogenous in all directions at
266 that scale, especially over varying terrain. So, for example, the coarse resolution of the model,
267 even with added measurements is likely not accurately capturing the gradient between coastal
268 and inland deposition. While higher resolution precipitation values are available in some regions
269 (e.g. PRISM in the US), there is still a dearth of both wet and dry deposition measurements.
270 Schwede et al. (Schwede et al., 2011) showed that dry deposition estimates from CASTNET and
271 CAPMoN can be very different, despite using similar methodologies. This adds uncertainty to
272 the dry deposition data (though there are very few dry deposition estimates included in this
273 study) and emphasizes the importance of deposition velocity model methodology.

274 The differences between the TDep, MMM, and MMF gridded deposition in the US (Figure 5)
275 are clear on the coasts. While the general patterns of deposition are similar for the three products,
276 the magnitude of deposition in the aggregated TDep dataset (1^o x 1^o) is higher in the eastern US
277 and lower in the western US than either of the other two deposition fields. This difference is
278 likely due to the precipitation dataset used to calculate wet deposition. MMF deposition is based
279 on the MMM dataset; therefore, both utilize the same precipitation dataset, from a combination
280 of 11 global models. However, TDep wet deposition is produced by multiplying PRISM
281 precipitation data and an interpolated gridded surface dataset of wet NH₄⁺ concentrations.
282 PRISM is a reanalysis product designed to interpolate precipitation in particularly complex



283 landscapes using weather radar and rainfall gauge observations, though it is not identical to
284 observations because it used long-term averages as predictor grids (Zhang et al., 2018). It
285 captures much more localized variation in precipitation due to geographical variations which are
286 not captured in the lower resolution global precipitation models used in the HTAP II MMM (Tan
287 et al., 2018). To illustrate this, we compare PRISM to the available Community Atmosphere
288 Model with Chemistry (<https://www2.aom.ucar.edu/gcm/cam-chem>, “CAM-Chem”), which
289 was one of the models in the HTAP II ensemble. Subtracting the CAM-Chem precipitation
290 output over the US from aggregated PRISM precipitation shows that CAM-Chem greatly
291 underestimates precipitation volume in the US in 2010 (Figure S1). We note, however, that this
292 comparison does not take precipitation frequency into account. This matters because if the
293 difference in volume comes from a few large magnitude storms, it will not influence the
294 deposition values much. This is a good example of the differences that occur when comparing
295 global and regional climate models and serves to emphasize the importance of resolving spatial
296 and temporal scales. The total deposition within the US borders is similar for the MMF, HTAP
297 II, and aggregated TDep gridded surfaces; however, the spatial distribution is different.

298 MMF and MMM deposition distributions are similar because MMF is based on HTAP II.
299 Likewise, the MMF results are similar to the TDep values at observation locations because,
300 despite the difference in precipitation, both utilize the same NADP/NTN measurements to
301 constrain the models. The key difference between MMF, when compared to MMM, is that
302 measurement locations are not centered in each $1^{\circ} \times 1^{\circ}$ grid cell; therefore, the center of each
303 grid cell (the value compared to the observation, by interpolation to the station location) will not
304 exactly equal the measured deposition but will instead be equal to the measurements weighted
305 proportionally to distance from the centroid. This means that the graphical comparison of Figure
306 6 is showing the actual measurement locations and 3 different model results with some
307 meaningful influence from measurements that are nonetheless unique values, except in the very
308 rare instance that the measurement corresponds exactly to the center of a grid cell.

309 TDep maps of North American nitrogen deposition created with Schwede and Lear’s
310 methodology (2014), using IDW, are widely in use and freely available from the NADP.
311 However, there are limitations associated with IDW (Sahu et al., 2010), and other interpolation
312 methods such as kriging or geographically weighted regression could provide smoother surfaces
313 with fewer artifacts. IDW is a fast and flexible interpolation method, but it does not minimize



314 error and can produce inaccurate results in regions with sparse measurements and large sub-grid
315 variability. This problem is relevant to much of the world. The lack of measurement sites
316 globally is a hindrance that can be alleviated by including remotely sensed observations (Walker
317 et al., 2019). Future work should also investigate methods such as machine learning techniques
318 with spatial information to avoid these limitations.

319 These results from measurement-model fusion are important because previous methods on a
320 global scale have relied primarily on models (Vet et al., 2014; Tan et al., 2018). They compare
321 their results with measurements, of course, in order to demonstrate the model capabilities but
322 they do not explicitly incorporate point measurements into the final product. Our results serve to
323 emphasize that the models are adequately simulating deposition (in terms of total deposition
324 budgets) but that the regional discrepancies between models and measurements can still be quite
325 large; and measurement-model fusion helps to ameliorate this without changing the fundamental
326 model parameters and processes that actually capture the overall deposition reasonably well.

327 **6. Conclusions**

328 Sulfur and nitrogen depositions remain a serious concern for human and ecosystem health. We
329 update the 2010 deposition budgets using measurement-model fusion to combine the broad
330 spatial coverage of a model with accurate in-situ measurements. The total nitrogen deposition
331 budget is recalculated to 130 Tg-N and the sulfur budget is 80 Tg-N, representing about a 10%
332 increase and no change, respectively, from the modeled values. This work emphasizes the
333 necessity of combining models with observations wherever possible to better capture regional
334 patterns and to inform policy and decision-making. Future work to improve measurement-model
335 fusion should investigate other methods of interpolation to avoid the limitations associated with
336 IDW such as surface artifacts and high error in regions with sparse measurements. It should also
337 incorporate satellite imagery to improve model estimates where in-situ measurements are not
338 available.



339 **Author Contribution**

340 HR carried out the methods and analyzed the results. JSF and FD designed the project. HR
341 prepared the manuscript with contributions from JSF and FD. RL, KH, and HF provided data.

342 **Competing Interests**

343 The authors declare no competing interests.

344 **Code Availability**

345 Data analysis was done using ArcMap Desktop 10.8.1, ArcGIS Pro, and R (R Core Team, 2022).

346



347 **References**

- 348 Adon, M., Galy-Lacaux, C., Yoboué, V., Delon, C., Lacaux, J. P., Castera, P., Gardrat, E.,
349 Pienaar, J., Al Ourabi, H., Laouali, D., Diop, B., Sigha-Nkamdjou, L., Akpo, A., Tathy, J. P.,
350 Lavenu, F., and Mougin, E.: Long term measurements of sulfur dioxide, nitrogen dioxide,
351 ammonia, nitric acid and ozone in Africa using passive samplers, *Atmos. Chem. Phys.*, 10,
352 7467–7487, <https://doi.org/10.5194/acp-10-7467-2010>, 2010.
- 353 Anderson, D. M., Burkholder, J. M., Cochlan, W. P., Glibert, P. M., Gobler, C. J., Heil, C. A.,
354 Kudela, R. M., Parsons, M. L., Rensel, J. E. J., Townsend, D. W., Trainer, V. L., and Vargo, G.
355 A.: Harmful algal blooms and eutrophication: Examining linkages from selected coastal regions
356 of the United States, *Harmful Algae*, 8, 39–53, <https://doi.org/10.1016/j.hal.2008.08.017>, 2008.
- 357 Acid Deposition Monitoring Network in East Asia (EANET): <https://www.eanet.asia/>, last
358 access: 18 November 2021.
- 359 Bobbink, R., Hicks, K., Galloway, J., Spranger, T., Alkemade, R., Ashmore, M., Bustamante,
360 M., Cinderby, S., Davidson, E., Dentener, F., Emmett, B., Erisman, J.-W., Fenn, M., Gilliam, F.,
361 Nordin, A., Pardo, L., and Vries, W. D.: Global assessment of nitrogen deposition effects on
362 terrestrial plant diversity: a synthesis, *Ecological Applications*, 20, 30–59,
363 <https://doi.org/10.1890/08-1140.1>, 2010.
- 364 Bowman, W. D., Cleveland, C. C., Halada, L., Hreško, J., and Baron, J. S.: Negative impact of
365 nitrogen deposition on soil buffering capacity, *Nature Geoscience*, 1, 767–770,
366 <https://doi.org/10.1038/ngeo339>, 2008.
- 367 Clark, C. M., Bai, Y., Bowman, W. D., Cowles, J. M., Fenn, M. E., Gilliam, F. S., Phoenix, G.
368 K., Siddique, I., Stevens, C. J., Sverdrup, H. U., and Throop, H. L.: Nitrogen Deposition and
369 Terrestrial Biodiversity, in: *Encyclopedia of Biodiversity*, Elsevier, 519–536,
370 <https://doi.org/10.1016/B978-0-12-384719-5.00366-X>, 2013.
- 371 Dentener, F., Drevet, J., Lamarque, J. F., Bey, I., Eickhout, B., Fiore, A. M., Hauglustaine, D.,
372 Horowitz, L. W., Krol, M., Kulshrestha, U. C., Lawrence, M., Galy-Lacaux, C., Rast, S.,
373 Shindell, D., Stevenson, D., Noije, T. V., Atherton, C., Bell, N., Bergman, D., Butler, T., Cofala,
374 J., Collins, B., Doherty, R., Ellingsen, K., Galloway, J., Gauss, M., Montanaro, V., Müller, J. F.,
375 Pitari, G., Rodriguez, J., Sanderson, M., Solomon, F., Strahan, S., Schultz, M., Sudo, K., Szopa,
376 S., and Wild, O.: Nitrogen and sulfur deposition on regional and global scales: A multimodel
377 evaluation, *Global Biogeochemical Cycles*, 20, <https://doi.org/10.1029/2005GB002672>, 2006.
- 378 Dise, N. B. and Stevens, J.: Nitrogen deposition and reduction of terrestrial biodiversity:
379 Evidence from temperate grasslands, *Sci. China Ser. C-Life Sci.*, 48, 720–728,
380 <https://doi.org/10.1007/BF03187112>, 2005.
- 381 Doney, S. C., Mahowald, N., Lima, I., Feely, R. A., Mackenzie, F. T., Lamarque, J.-F., and
382 Rasch, P. J.: Impact of anthropogenic atmospheric nitrogen and sulfur deposition on ocean
383 acidification and the inorganic carbon system, *PNAS*, 104, 14580–14585,
384 <https://doi.org/10.1073/pnas.0702218104>, 2007.



- 385 European Monitoring and Evaluation Programme (EMEP): <https://www.emep.int/>, last access: 18
386 November 2021.
- 387 Canadian Air and Precipitation Monitoring Network: <https://www.canada.ca/en/environment-climate-change/services/air-pollution/monitoring-networks-data/canadian-air-precipitation.html>,
388 last access: 18 November 2021.
389
- 390 Fu, J. S., Carmichael, G. R., Dentener, F., Aas, W., Andersson, C., Barrie, L. A., Cole, A., Galy-
391 Lacaux, C., Geddes, J., Itahashi, S., Kanakidou, M., Labrador, L., Paulot, F., Schwede, D., Tan,
392 J., and Vet, R.: Improving Estimates of Sulfur, Nitrogen, and Ozone Total Deposition through
393 Multi-Model and Measurement-Model Fusion Approaches, *Environ. Sci. Technol.*, 56, 2134–
394 2142, <https://doi.org/10.1021/acs.est.1c05929>, 2022.
- 395 Galy-Lacaux, C., Delon, C., Solmon, F., Adon, M., Yoboué, V., Mphepya, J., Pienaar, J. J.,
396 Diop, B., Sigha, L., Dungall, L., Akpo, A., Mougou, E., Gardrat, E., and Castera, P.: Dry and Wet
397 Atmospheric Nitrogen Deposition in West Central Africa, in: *Nitrogen Deposition, Critical
398 Loads and Biodiversity*, edited by: Sutton, M. A., Mason, K. E., Sheppard, L. J., Sverdrup, H.,
399 Haeuber, R., and Hicks, W. K., Springer Netherlands, Dordrecht, 83–91,
400 https://doi.org/10.1007/978-94-007-7939-6_10, 2014.
- 401 Geddes, J. A. and Martin, R. V.: Global deposition of total reactive nitrogen oxides from 1996 to
402 2014 constrained with satellite observations of NO₂ columns, *Atmospheric Chemistry and
403 Physics*, 17, 10071–10091, <https://doi.org/10.5194/acp-17-10071-2017>, 2017.
- 404 Heisler, J., Glibert, P. M., Burkholder, J. M., Anderson, D. M., Cochlan, W., Dennison, W. C.,
405 Dortch, Q., Gobler, C. J., Heil, C. A., Humphries, E., Lewitus, A., Magnien, R., Marshall, H. G.,
406 Sellner, K., Stockwell, D. A., Stoecker, D. K., and Suddleson, M.: Eutrophication and harmful
407 algal blooms: A scientific consensus, *Harmful Algae*, 8, 3–13,
408 <https://doi.org/10.1016/j.hal.2008.08.006>, 2008.
- 409 INDAAF – International Network to study Deposition and Atmospheric chemistry in Africa:
410 <https://indaaf.obs-mip.fr/>, last access: 18 November 2021.
- 411 Jia, Y., Yu, G., He, N., Zhan, X., Fang, H., Sheng, W., Zuo, Y., Zhang, D., and Wang, Q.:
412 Spatial and decadal variations in inorganic nitrogen wet deposition in China induced by human
413 activity, *Sci Rep*, 4, 3763, <https://doi.org/10.1038/srep03763>, 2014.
- 414 Kicklighter, D. W., Melillo, J. M., Monier, E., Sokolov, A. P., and Zhuang, Q.: Future nitrogen
415 availability and its effect on carbon sequestration in Northern Eurasia, *Nat Commun*, 10, 3024,
416 <https://doi.org/10.1038/s41467-019-10944-0>, 2019.
- 417 Labrador, L., Volosciuk, C., and Cole, A.: Measurement-Model Fusion for Global Total
418 Atmospheric Deposition, a WMO initiative, World Meteorological Organization, 2020.
- 419 Lamarque, J.-F., Dentener, F., McConnell, J., Ro, C.-U., Shaw, M., Vet, R., Bergmann, D.,
420 Cameron-Smith, P., Dalsoren, S., Doherty, R., Faluvegi, G., Ghan, S. J., Josse, B., Lee, Y. H.,
421 MacKenzie, I. A., Plummer, D., Shindell, D. T., Skeie, R. B., Stevenson, D. S., Strode, S., Zeng,
422 G., Curran, M., Dahl-Jensen, D., Das, S., Fritzsche, D., and Nolan, M.: Multi-model mean



- 423 nitrogen and sulfur deposition from the Atmospheric Chemistry and Climate Model
424 Intercomparison Project (ACCMIP): evaluation of historical and projected future changes,
425 *Atmos. Chem. Phys.*, 13, 7997–8018, <https://doi.org/10.5194/acp-13-7997-2013>, 2013.
- 426 Li, R., Cui, L., Zhao, Y., Zhang, Z., Sun, T., Li, J., Zhou, W., Meng, Y., Huang, K., and Fu, H.:
427 Wet deposition of inorganic ions in 320 cities across China: spatio-temporal variation, source
428 apportionment, and dominant factors, *Atmospheric Chemistry and Physics*, 19, 11043–11070,
429 <https://doi.org/10.5194/acp-19-11043-2019>, 2019.
- 430 Liu, L., Zhang, X., Xu, W., Liu, X., Zhang, Y., Li, Y., Wei, J., Lu, X., Wang, S., Zhang, W.,
431 Zhao, L., Wang, Z., and Wu, X.: Fall of oxidized while rise of reduced reactive nitrogen
432 deposition in China, *Journal of Cleaner Production*, 272, 122875,
433 <https://doi.org/10.1016/j.jclepro.2020.122875>, 2020.
- 434 Lu, Z., Streets, D. G., Zhang, Q., Wang, S., Carmichael, G. R., Cheng, Y. F., Wei, C., Chin, M.,
435 Diehl, T., and Tan, Q.: Sulfur dioxide emissions in China and sulfur trends in East Asia since
436 2000, *Atmos. Chem. Phys.*, 10, 6311–6331, <https://doi.org/10.5194/acp-10-6311-2010>, 2010.
- 437 Luo, X. S., Tang, A. H., Shi, K., Wu, L. H., Li, W. Q., Shi, W. Q., Shi, X. K., Erisman, J. W.,
438 Zhang, F. S., and Liu, X. J.: Chinese coastal seas are facing heavy atmospheric nitrogen
439 deposition, *Environ. Res. Lett.*, 9, 095007, <https://doi.org/10.1088/1748-9326/9/9/095007>, 2014.
- 440 National Atmospheric Deposition Program: <https://nadp.slh.wisc.edu/>, last access: 18 November
441 2021.
- 442 Qu, L., Xiao, H., Zheng, N., Zhang, Z., and Xu, Y.: Comparison of four methods for spatial
443 interpolation of estimated atmospheric nitrogen deposition in South China, *Environ Sci Pollut*
444 *Res.*, 24, 2578–2588, <https://doi.org/10.1007/s11356-016-7995-0>, 2017.
- 445 R Core Team: *R: A Language and Environment for Statistical Computing*, 2022.
- 446 Sahu, S. K., Gelfand, A. E., and Holland, D. M.: Fusing point and areal level space–time data
447 with application to wet deposition, *Journal of the Royal Statistical Society: Series C (Applied*
448 *Statistics)*, 59, 77–103, <https://doi.org/10.1111/j.1467-9876.2009.00685.x>, 2010.
- 449 Schwede, D., Zhang, L., Vet, R., and Lear, G.: An intercomparison of the deposition models
450 used in the CASTNET and CAPMoN networks, *Atmospheric Environment*, 45, 1337–1346,
451 <https://doi.org/10.1016/j.atmosenv.2010.11.050>, 2011.
- 452 Schwede, D., Cole, A., Vet, R., and Lear, G.: Ongoing U.S. - Canada Collaboration on Nitrogen
453 and Sulfur Deposition, 5, 2019.
- 454 Schwede, D. B. and Lear, G. G.: A novel hybrid approach for estimating total deposition in the
455 United States, *Atmospheric Environment*, 92, 207–220,
456 <https://doi.org/10.1016/j.atmosenv.2014.04.008>, 2014.



- 457 Sirois, A.: The effects of missing data on the calculation of precipitation-weighted-mean
458 concentrations in wet deposition, *Atmospheric Environment. Part A. General Topics*, 24, 2277–
459 2288, [https://doi.org/10.1016/0960-1686\(90\)90321-D](https://doi.org/10.1016/0960-1686(90)90321-D), 1990.
- 460 Tan, J., Fu, J. S., Dentener, F., Sun, J., Emmons, L., Tilmes, S., Sudo, K., Flemming, J., Jonson,
461 J. E., Gravel, S., Bian, H., Davila, Y., Henze, D. K., Lund, M. T., Kucsera, T., Takemura, T., and
462 Keating, T.: Multi-model study of HTAP II on sulfur and nitrogen deposition, *Atmospheric
463 Chemistry and Physics*, 18, 6847–6866, <https://doi.org/10.5194/acp-18-6847-2018>, 2018.
- 464 Tørseth, K., Aas, W., Breivik, K., Fjæraa, A. M., Fiebig, M., Hjellbrekke, A. G., Lund Myhre,
465 C., Solberg, S., and Yttri, K. E.: Introduction to the European Monitoring and Evaluation
466 Programme (EMEP) and observed atmospheric composition change during 1972 - 2009,
467 *Atmospheric Chemistry and Physics*, 12, 5447–5481, <https://doi.org/10.5194/acp-12-5447-2012>,
468 2012.
- 469 Clean Air Status and Trends Network (CASTNET): <https://www.epa.gov/castnet>, last access: 18
470 November 2021.
- 471 Vet, R., Artz, R. S., Carou, S., Shaw, M., Ro, C.-U., Aas, W., Baker, A., Bowersox, V. C.,
472 Dentener, F., Galy-Lacaux, C., Hou, A., Pienaar, J. J., Gillett, R., Forti, M. C., Gromov, S., Hara,
473 H., Khodzher, T., Mahowald, N. M., Nickovic, S., Rao, P. S. P., and Reid, N. W.: A global
474 assessment of precipitation chemistry and deposition of sulfur, nitrogen, sea salt, base cations,
475 organic acids, acidity and pH, and phosphorus, *Atmospheric Environment*, 93, 3–100,
476 <https://doi.org/10.1016/j.atmosenv.2013.10.060>, 2014.
- 477 de Vries, W., Solberg, S., Dobbertin, M., Sterba, H., Laubhann, D., van Oijen, M., Evans, C.,
478 Gundersen, P., Kros, J., Wamelink, G. W. W., Reinds, G. J., and Sutton, M. A.: The impact of
479 nitrogen deposition on carbon sequestration by European forests and heathlands, *Forest Ecology
480 and Management*, 258, 1814–1823, <https://doi.org/10.1016/j.foreco.2009.02.034>, 2009.
- 481 Walker, J. T., Beachley, G., Amos, H. M., Baron, J. S., Bash, J., Baumgardner, R., Bell, M. D.,
482 Benedict, K. B., Chen, X., Clow, D. W., Cole, A., Coughlin, J. G., Cruz, K., Daly, R. W.,
483 Decina, S. M., Elliott, E. M., Fenn, M. E., Ganzeveld, L., Gebhart, K., Isil, S. S., Kerschner, B.
484 M., Larson, R. S., Lavery, T., Lear, G. G., Macy, T., Mast, M. A., Mishoe, K., Morris, K. H.,
485 Padgett, P. E., Pouyat, R. V., Puchalski, M., Pye, H. O. T., Rea, A. W., Rhodes, M. F., Rogers,
486 C. M., Saylor, R., Scheffe, R., Schichtel, B. A., Schwede, D. B., Sexstone, G. A., Sive, B. C.,
487 Sosa Echeverría, R., Templer, P. H., Thompson, T., Tong, D., Wetherbee, G. A., Whitlow, T. H.,
488 Wu, Z., Yu, Z., and Zhang, L.: Toward the improvement of total nitrogen deposition budgets in
489 the United States, *Science of The Total Environment*, 691, 1328–1352,
490 <https://doi.org/10.1016/j.scitotenv.2019.07.058>, 2019.
- 491 Wen, Z., Xu, W., Li, Q., Han, M., Tang, A., Zhang, Y., Luo, X., Shen, J., Wang, W., Li, K., Pan,
492 Y., Zhang, L., Li, W., Collett, J. L., Zhong, B., Wang, X., Goulding, K., Zhang, F., and Liu, X.:
493 Changes of nitrogen deposition in China from 1980 to 2018, *Environment International*, 144,
494 106022, <https://doi.org/10.1016/j.envint.2020.106022>, 2020.
- 495 Xu, W., Luo, X. S., Pan, Y. P., Zhang, L., Tang, A. H., Shen, J. L., Zhang, Y., Li, K. H., Wu, Q.
496 H., Yang, D. W., Zhang, Y. Y., Xue, J., Li, W. Q., Li, Q. Q., Tang, L., Lu, S. H., Liang, T.,



- 497 Tong, Y. A., Liu, P., Zhang, Q., Xiong, Z. Q., Shi, X. J., Wu, L. H., Shi, W. Q., Tian, K., Zhong,
498 X. H., Shi, K., Tang, Q. Y., Zhang, L. J., Huang, J. L., He, C. E., Kuang, F. H., Zhu, B., Liu, H.,
499 Jin, X., Xin, Y. J., Shi, X. K., Du, E. Z., Dore, A. J., Tang, S., Collett, J. L., Goulding, K., Sun,
500 Y. X., Ren, J., Zhang, F. S., and Liu, X. J.: Quantifying atmospheric nitrogen deposition through
501 a nationwide monitoring network across China, *Atmos. Chem. Phys.*, 15, 12345–12360,
502 <https://doi.org/10.5194/acp-15-12345-2015>, 2015.
- 503 Xu, W., Zhang, L., and Liu, X.: A database of atmospheric nitrogen concentration and deposition
504 from the nationwide monitoring network in China, *Sci Data*, 6, 51,
505 <https://doi.org/10.1038/s41597-019-0061-2>, 2019.
- 506 Zhang, M., Leon, C. de, and Migliaccio, K.: Evaluation and comparison of interpolated gauge
507 rainfall data and gridded rainfall data in Florida, USA, *Hydrological Sciences Journal*, 63, 561–
508 582, <https://doi.org/10.1080/02626667.2018.1444767>, 2018.
- 509 Zhang, Y., Foley, K. M., Schwede, D. B., Bash, J. O., Pinto, J. P., and Dennis, R. L.: A
510 Measurement-Model Fusion Approach for Improved Wet Deposition Maps and Trends, *Journal*
511 *of Geophysical Research: Atmospheres*, 124, 4237–4251,
512 <https://doi.org/10.1029/2018JD029051>, 2019.
- 513 Zhao, Y., Zhang, L., Chen, Y., Liu, X., Xu, W., Pan, Y., and Duan, L.: Atmospheric nitrogen
514 deposition to China: A model analysis on nitrogen budget and critical load exceedance,
515 *Atmospheric Environment*, 153, 32–40, <https://doi.org/10.1016/j.atmosenv.2017.01.018>, 2017.
- 516 Zhu, J., Chen, Z., Wang, Q., Xu, L., He, N., Jia, Y., Zhang, Q., and Yu, G.: Potential transition in
517 the effects of atmospheric nitrogen deposition in China, *Environmental Pollution*, 258, 113739,
518 <https://doi.org/10.1016/j.envpol.2019.113739>, 2020.
- 519